



Assembly mechanism and photoproduced electron transfer for a novel cubic Cu₂O/tetrakis(4-hydroxyphenyl)porphyrin hybrid with visible photocatalytic activity for hydrogen evolution

Riyue Ge ^{a,1}, Xiangqing Li ^{a,*1}, Bing Zhuang ^a, Shi-Zhao Kang ^a, Lixia Qin ^a, Guodong Li ^b

^a School of Chemical and Environmental Engineering, Shanghai Institute of Technology, 100 Haiquan Road, Shanghai 201418, China

^b State Key Laboratory of Inorganic Synthesis and Preparative Chemistry, College of Chemistry, Jilin University, Changchun 130012, China



ARTICLE INFO

Article history:

Received 17 January 2017

Received in revised form 6 April 2017

Accepted 21 April 2017

Available online 23 April 2017

Keywords:

Porphyrin

Composite photocatalyst

Hydrogen evolution

Electron transfer

Mechanism

ABSTRACT

A novel composite with special structure and excellent performance, 5,10,15,20-tetrakis(4-hydroxyphenyl) porphyrin (THPP) coated Cu₂O nanoparticle (Cu₂O/THPP), was facilely prepared by a simple method. UV-vis spectra, FTIR and fluorescence spectra were used to explore the interaction mechanism between THPP molecule and Cu₂O nanoparticle. The results demonstrated that the center of the THPP macrocycle could coordinate with Cu₂O, besides hydrogen bond and/or electrostatic interaction between peripheries of THPP macrocycle and Cu₂O. Furthermore, photocatalytic hydrogen evolution performance of the composite was investigated. The composite displayed more excellent performance for hydrogen evolution than that of pure THPP, pure Cu₂O or 5,10,15,20-tetraphenylporphyrin (TPP) coated Cu₂O nanoparticle (Cu₂O/TPP). By means of fluorescence spectra, electrochemical impedance spectra and photoelectronic performance measurement, the mechanism of electron transfer in the composite was explored. The results showed that the strong synergistic interaction caused by the special combination mode between THPP and Cu₂O can quicken the transfer of photo-generated electrons, and was very favorable to improve the performance of the Cu₂O/THPP composite.

© 2017 Elsevier B.V. All rights reserved.

1. Introduction

Hydrogen energy is considered to be an environment-friendly energy replacing fossil fuels. In technologies of hydrogen evolution, photocatalytic water reduction by semiconductor-based photocatalysts is one of the efficient ways. In those photocatalysts, the nanostructured photocatalysts with low-cost and high activity have attracted considerable interest of the researchers [1].

Due to cheap cost and good performance, some transition metal oxides have been the research focus in the fields of catalysis, water treatment and sensors [2–4]. Cuprous oxide is a kind of typical p-type oxide semiconductor, and shows potential applications in solar energy conversion and catalysis, especially, in water splitting and the degradation of organic dyes [5]. For example, by loading Au nanoparticles on the surface of Cu₂O, Mahmoud and his coworkers have achieved an efficient catalyst for the degradation of Rhodamine B [6]. However, the application of Cu₂O is limited due to

easier corrosion and lower activity. Constructing hybrid structures [7], coupling with some semiconductors [8] or controlling morphology [9] is the efficient way to solve these problems. In various Cu₂O, the Cu₂O with cubic structure is vital because many other forms of Cu₂O crystals could derive from this one [10].

The metal oxide based hybrid photocatalysts with higher visible light absorption are important for improving their activities for hydrogen evolution. Porphyrins possess adjustable structure, high molar extinction coefficient and excellent photoelectrochemical properties, and have been used in constructing metal-based or metal oxide-based hybrid structures for energy harvesting, water splitting, pollutant photodegradation and sensor [11,12]. Marczał et al. combined two kinds of porphyrin molecules (DOPAZ and CAMIZ) with ZnO nanoparticles, and prepared a porphyrin/ZnO nanoparticles composite with high visible light absorption [13]. It is reported that hydroxyphenyl functional groups at the meso positions of porphyrin molecule can enhance the intermolecular interaction and self-assembly properties via hydrogen bonding [14,15]. To understand the relationship between synergistic interplay of noncovalent interactions in controlling and tuning the morphology of nanostructures of porphyrin derivatives, it is important to prepare novel porphyrin-based nanocomposite.

* Corresponding author.

E-mail address: xqli@sit.edu.cn (X. Li).

¹ The first two authors contributed equally to this paper.

Although the concept of dye sensitization is not new, photofunctional systems composed of the porphyrin with special structure and the cubic Cu_2O are critically lack. Moreover, electron transfer from photo-excited porphyrins to a variety of acceptor moieties is also interested [16]. Assembly and electron transfer mechanisms of porphyrins and the cubic Cu_2O still need to be studied.

Herein, with 5,10,15,20-tetrakis(4-hydroxyphenyl) porphyrin (THPP) acting as light trapper and electron donor, Cu_2O acting as electron acceptor and active center, a novel $\text{Cu}_2\text{O}/\text{THPP}$ composite with special structure is prepared by a facile method. The interaction mechanism between Cu_2O and THPP is studied. Moreover, the performances of photoelectronic response and photocatalytic hydrogen evolution for the nanocomposite are investigated. The mechanism of electron transfer is investigated in detail. Using THPP molecules for surface functionalization of Cu_2O will provide additional control for surface loading and attachment stability of porphyrins on metal oxides based photocatalysts.

2. Experimental section

2.1. Materials

5,10,15,20-tetrakis(4-hydroxyphenyl) porphyrin (THPP) (~95%) and 5,10,15,20-tetraphenylporphyrin (TPP) (~97%) were purchased from J&K Scientific. CuTPP and CuTHPP were prepared according to the literature reported [17]. Triethanolamine (TEA), $\text{CuCl}_2 \cdot 2\text{H}_2\text{O}$, polyethylene glycol (PEG) and NaOH were of analytical reagent (A.R.), and were bought from Sinopharm Chemical Reagent Co. The other chemicals were of analytical reagent and used without further purification.

2.2. Preparation of Cu_2O

Firstly, 1.6 g PEG (M_w : 10000) was dissolved into deionized water (500 mL) and ultra-sounded for 30 min. Then, 612 mg of $\text{CuCl}_2 \cdot 2\text{H}_2\text{O}$ was added into the mixture and stirred for 30 min. Afterwards, 1.15 g of NaOH was gradually added into the above mixture, and stirred for another 10 min. 0.73 mL of hydrazine hydrate (N_2H_4) was added slowly into the above mixture. When the color of the mixture became from blue to brownish red, the mixture was filtered. The precipitate was washed with deionized water for several times. Subsequently, the Cu_2O was obtained.

2.3. Preparation of the $\text{Cu}_2\text{O}/\text{THPP}$ composite

A certain amount of THPP was dissolved in ethanol and refluxed for about 1 h. Cu_2O was added into the THPP solution (The mass ratio of Cu_2O to THPP was 1%, 5%, 10%, 25% and 50%, respectively.). The reaction was monitored by UV-vis spectrum. When UV-vis spectra of the solution did not change any more, the reaction was stopped. Then, the mixture was transferred into a culture dish, and dried in a vacuum oven at 60 °C. Substituted THPP with TPP, $\text{Cu}_2\text{O}/\text{TPP}$ composite was obtained by similar procedure. According to the preparation process of the $\text{Cu}_2\text{O}/\text{THPP}$ composite, THPP and Cu_2O were hardly lost. That is, the theoretical ratio of Cu_2O to THPP was almost equal to the actual ratio. Therefore, the ratio of Cu_2O to THPP was not further ascertained with thermogravimetric analysis.

2.4. Measurement of photoelectric performance

First, FTO glasses were cleaned by sonication in ethanol, acetone, chloroform and double distilled water for 15 min, respectively, and then dried in the atmosphere. Fluorine-doped tin oxide (FTO) glasses coated with the sample were used as working electrodes. They were prepared via the following procedure. In brief, 10 mg

of the sample was added into 2 mL of alcohol, and the mixture was sonicated for 30 s. After that, the FTO glass ($1 \times 1.5 \text{ cm}^2$) was soaked into the slurry for 1 min, and pulled out and heat-treated at 60 °C for 1 h. The photoelectrochemical and electrochemical impedance measurements were carried out at room temperature using Chenhua CHI 660E computer controlled electrochemical analyzer with a standard three-electrode system. Ag/AgCl electrode was used as the reference electrode, and a platinum wire was used as the counter electrode. The electrolyte was 0.5 mol L⁻¹ of Na_2SO_4 aqueous solution, and the air in the solution was removed by purging N_2 for 15 min.

2.5. Measurement of photocatalytic activity

The photocatalytic hydrogen evolution over the samples was performed through a CEL-SP2N water splitting system (Fig. S1, Zhongjiao Jinyuan Instruments, China) with a 300 W Xe lamp as the light source. In detail, 10 mg of the sample was dispersed into 60 mL of 10 vol.% TEA aqueous solution. The reaction temperature was kept at about 8.5 °C by circulating water jacket. Before irradiation, it was evacuated by a vacuum pump in order to remove the air in the system. The H_2 evolved was analyzed by a continuous online gas chromatography (AULTT Co., Beijing) equipped with a thermal conductivity detector, and the high-purity N_2 (99.999%) was used as the carrier gas.

2.6. Characterizations

UV-vis absorption spectra were measured with a UV-3900 spectrophotometer (Japan). Fourier transform infrared spectra (FTIR) were recorded on a Nicolet 6700 FTIR spectrometer (USA). Transmission electron microscope (TEM) images were taken with the JEOL JEM-2100F microscope device (Japan), and the accelerating voltage was 200 kV. X-ray photoelectron spectra (XPS) were measured on a Thermo ESCALAB 250 X-ray photoelectron spectrometer with a monochromatic X-ray source ($\text{Al K}_\alpha h\nu = 1486.6 \text{ eV}$) (USA). X-ray powder diffraction (XRD) was carried out using a Bruker D8 Advance X-ray diffractometer (Germany). Fluorescence spectra were carried out using an F-4600 fluorescence spectrophotometer (Japan).

3. Results and discussion

3.1. Assembly mechanism of Cu_2O and THPP

UV-vis spectroscopy is one of the important means to understand the interaction on the interface, surface composition and coordination geometry. In order to explore the interaction mechanism of Cu_2O and THPP, UV-vis spectra of the THPP solution and the THPP solution added Cu_2O are measured. Because the molar extinction coefficient of the Soret band is much larger than those of the Q bands, the Q bands are hardly observed in Fig. 1a, and the position of the Soret band is not distinct either. In order to observe them more clearly, the Soret band and Q bands in different range of the absorbance are provided, respectively (Fig. 1b and c). As shown in Fig. 1a and Fig. 1b, a Soret band at 419 nm is observed for the THPP solution (the solid lines), which arises from $a_{1u}(\pi)$ to $e_g^*(\pi)$ transition. Besides, four weak bands at 515 nm, 553 nm, 595 nm and 650 nm are attributed to Q bands arising from $a_{2u}(\pi)$ to $e_g^*(\pi)$ transition (Fig. 1a and c, the solid lines). After introducing 5% Cu_2O into the THPP solution and reacting for 4 h, the Soret band at 419 nm disappears, and a new band at 415 nm appears. Besides, the number of Q bands is reduced to two, and it locates at about 539 nm and 579 nm, respectively. The phenomenon is the important proof for metallation of porphyrin macrocycle [18]. Therefore,

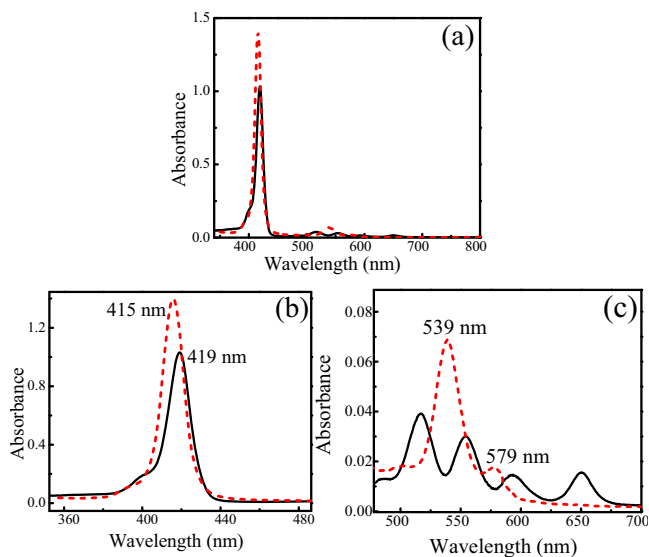


Fig. 1. UV-vis spectra of THPP ethanol solution after adding 5%Cu₂O and reacting at 78 °C for 0 h (the solid lines) and 4 h (the dotted lines). (a): UV-vis spectra in the range of 340–800 nm; (b): UV-vis spectra in the range of 353–486 nm (Observe the Soret band more clearly); (c): UV-vis spectra in the range of 486–700 nm (Observe the Q bands more clearly).

it is deduced that the coordination interaction takes place between THPP macrocycle and the Cu₂O.

Replaced THPP with TPP, UV-vis spectra of the TPP solution added Cu₂O is similar to that of the THPP solution added Cu₂O (Fig. S2). Differently, the reaction rate of Cu₂O and TPP is faster than that of Cu₂O and THPP. As can be seen in Fig. 2, the reaction time and the color of the solution are different for Cu₂O/TPP and Cu₂O/THPP, and have close relationships with the amount of Cu₂O in the porphyrin solution. The reaction time is shortened when the amount of Cu₂O in the porphyrin solution is increased. Compared with that of THPP and Cu₂O, the reaction time of TPP and Cu₂O is shorter at the same reaction conditions. In addition, the change in color of the TPP solution is more obvious after reacting with same amount of Cu₂O. For example, after adding 50% Cu₂O into TPP, the reaction is completed in 1 h, and the purplish color of the TPP solution almost disappears. However, in the same conditions, the reaction is com-

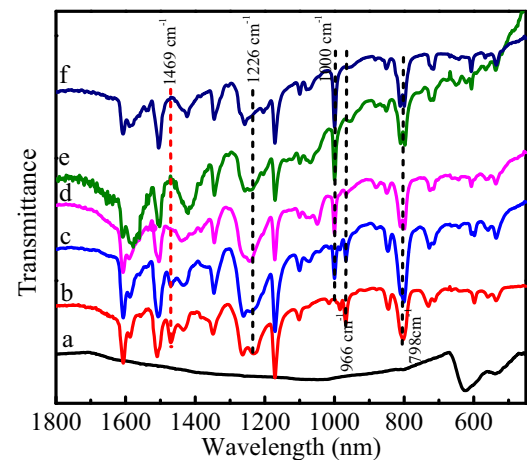


Fig. 3. FTIR spectra of Cu₂O (a), THPP (b), 3%Cu₂O/THPP (c), 5%Cu₂O/THPP (d), 10%Cu₂O/THPP (e) and 25%Cu₂O/THPP (f).

pleted in 2.5 h for THPP and Cu₂O, and the color of the THPP solution only becomes dark red. The differences from the reaction time and the color of the solution could be caused by the different combination model for the two porphyrins and Cu₂O. Because the THPP molecule contains four hydroxyl groups at its periphery, it could be linked first on the surface of Cu₂O by hydrogen bond and/or electrostatic interaction (between hydroxyl groups and copper ions), and then coordinated with Cu₂O by its macrocycle center with the Cu⁺ on the Cu₂O [19]. Subsequently, it needs longer reaction time. The special combination model for the THPP and Cu₂O was further demonstrated by FTIR (Fig. 3).

FTIR spectrum is a common and valid characterization method for exploring the change of functional groups and combination mode. FTIR spectra of various Cu₂O/THPP samples are shown in Fig. 3. For pure THPP, the band at 798 cm⁻¹ is ascribed to –OH bending vibration. After being introduced into Cu₂O, the band is blue-shifted to 811 cm⁻¹. It is the sign of the interaction between THPP and Cu₂O. In addition, the two bands at 1226 cm⁻¹ and 1469 cm⁻¹ (Fig. 3b) ascribed to the stretching vibration and deformation vibration of C–O and O–H [20], respectively, are also observed. When the amount of Cu₂O in the composite increases, the two bands disappear gradually. The above results could be caused

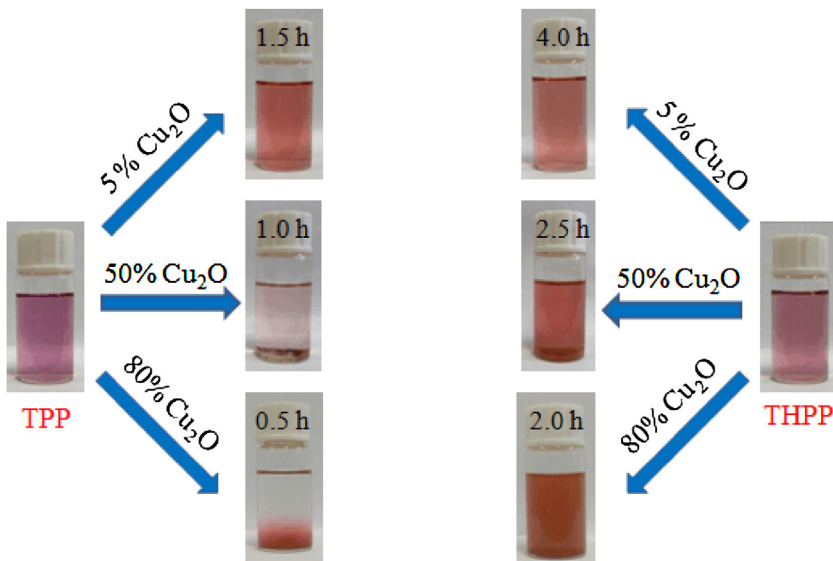
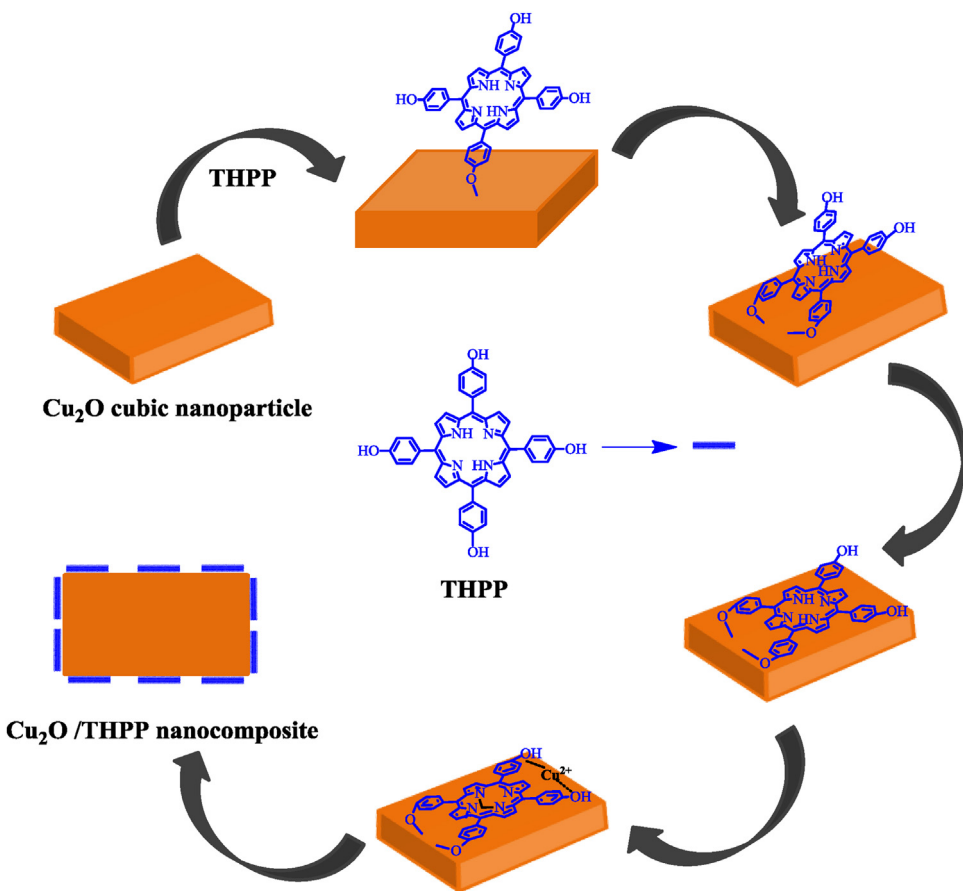


Fig. 2. The digital photos of 0.01 mg mL⁻¹ porphyrin (THPP/TPP) solution after adding various amount of Cu₂O and the corresponding reaction time at 78 °C.



Scheme 1. The proposed scheme illustrating the assembly of THPP and Cu₂O.

by the hydrogen bond among the hydroxyl groups located at the peripheries of THPP and those on the Cu₂O, or electrostatic interaction among the hydroxyl groups at the peripheries of THPP and copper ions on the Cu₂O. The band at 966 cm⁻¹ corresponds to the stretching vibration of C–N in the center of THPP (Fig. 3b). However, in the FTIR spectra of the Cu₂O/THPP composites (Fig. 3c–f), the band at 966 cm⁻¹ becomes weak gradually followed with increasing Cu₂O in the composite, and a new band at about 1000 cm⁻¹ appears, which is metallation characteristic of the THPP macrocycle [21]. It is similar to the FTIR spectrum of the Cu₂O/TPP (Fig. S3). It is indicated that the Cu⁺ enters the center of porphyrin macrocycle [22]. According to the above results, it is concluded that, besides hydrogen bond and/or electrostatic interaction, some THPP molecules are assembled on the Cu₂O through coordination interaction of Cu₂O and THPP macrocycle.

THPP molecule possesses a special structure (Scheme 1, four hydroxyl groups at the peripheries of the THPP macrocycle), which is different from that of TPP (Scheme S1). According to the results of UV–vis spectra and FTIR spectra, the possible assembly mechanism between Cu₂O and THPP is shown in Scheme 1. First, one of the hydroxyl groups at the THPP was linked with that of Cu₂O, and then electrostatic interaction takes place between hydroxyl groups at the THPP with the copper ions on the Cu₂O. When the center of the THPP macrocycle is close to the surface of the Cu₂O, the coordinate interaction takes place between the center of the THPP macrocycle and Cu⁺ on the Cu₂O, which will promote THPP molecules to flatten on the surface of Cu₂O and catalyze the metallation reaction of porphyrin macrocycles [23]. Therefore, it is deduced that more than one hydroxyl group react with Cu₂O. Otherwise, THPP macrocycle is difficult to coordinate with Cu₂O due to the disadvantageous configuration, and could not observe the metallation of

some THPP macrocycles in UV–vis spectra and FTIR. Obviously, the assembly between Cu₂O and THPP is different from that of Cu₂O and TPP (Scheme S1). The stronger interaction (hydrogen bond, electrostatic interaction and coordination interaction) between THPP and Cu₂O is profitable to improve the electron transfer efficiency.

3.2. Analysis of structure and morphology

XRD patterns of the samples are recorded and shown in Fig. 4A. In Fig. 4A (a), the diffraction peaks at $2\theta = 29.9^\circ, 36.8^\circ, 42.7^\circ, 61.8^\circ, 74.0^\circ$ and 77.8° correspond to (110), (111), (200), (220), (311) and (322) crystal planes, respectively, which coincide with those of the cubic phase Cu₂O (JCPDS card, No. 78-2076) [20]. After introducing Cu₂O into THPP, the peaks at $2\theta = 36.8^\circ, 61.8^\circ$ and 77.8° become weak, and the peaks at $2\theta = 42.7^\circ$ and 74.0° shift to 43.5° and 74.4° , respectively. In addition, a new peak at $2\theta = 50.6^\circ$ is observed. Referred to Asen's report [24], the peaks located at $43.5^\circ, 50.6^\circ$ and 74.4° (Fig. 4A (b)) correspond to the (111), (200) and (220) crystal faces of Cu(OH)₂, respectively. The small deviation of XRD peak positions between ours and Asens' could be ascribed to the generated oxygen vacancy or the change in lattice values [25], while no difference of the crystalline structure was observed between our result and Asen's report [24]. It is indicated that a small amounts of Cu(OH)₂ are formed on the surface of Cu₂O, which cover some crystal faces of Cu₂O. The Cu(OH)₂ could come from the surface oxidation of tiny amounts of Cu₂O (it can be confirmed by XPS spectra of Cu2p, Fig. 4B) and then the electrostatic interaction between the produced Cu²⁺ and hydroxyl groups of some THPP molecules. When the amount of Cu₂O in the composite is lower than 5% (Fig. 4A (c)), no obvious XRD peaks corresponding to Cu(OH)₂ or Cu₂O are

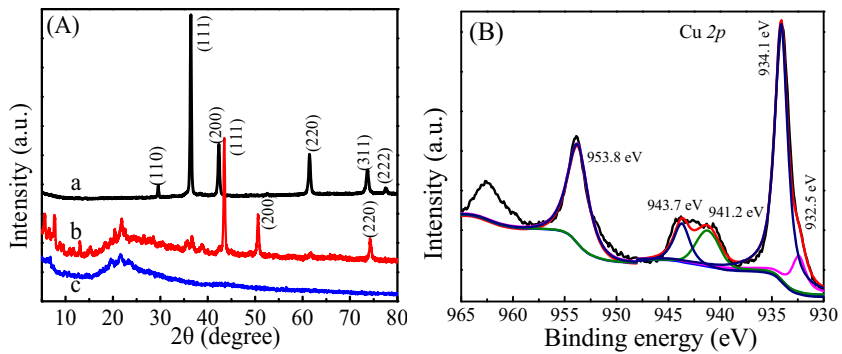


Fig. 4. (A) XRD spectra of Cu₂O (a), 25% Cu₂O/THPP (b) and 5% Cu₂O/THPP (c). (B) The high-resolution XPS spectra of Cu2p in 5% Cu₂O/THPP composite.

observed. It could be attributed to a low amount or good dispersion of Cu(OH)₂ or Cu₂O in the composite.

All samples were prepared by the same method. In order to verify the valence state of copper in the composite, the high-resolution XPS spectrum of Cu2p is measured. The high-resolution XPS spectra of Cu2p for the samples are similar. Herein, with 5% Cu₂O/THPP as a representative sample, its high-resolution XPS spectrum is shown in Fig. 4B. The binding energy attributed to Cu2p_{3/2} and Cu2p_{1/2} is located at 934.1 eV and 953.8 eV, respectively, which is the typical characteristic for Cu⁺ [26]. In addition, two satellite peaks (963 eV and 941.2–943.7 eV) corresponding to Cu²⁺ are also observed in Fig. 4B [27]. The Cu²⁺ detected by XPS could come from the surface oxidation of tiny amounts of Cu₂O [28]. Combined with the result of XRD (Fig. 4A), the Cu²⁺ detected on the surface of Cu₂O is in the form of Cu(OH)₂.

As shown in Fig. 5A, crosslinked nanoribbons can be observed in the TEM image of THPP. It is attributed to hydrogen bond interaction among hydroxyl groups in the THPP [29]. As can be seen in Fig. 5B, the Cu₂O nanoparticles possess cubic structure. After assembling with THPP, the microscopic network structure of the THPP in the composite are well-reflected by the observed structure, and the Cu₂O particles in the Cu₂O/THPP composite intertwined by crosslinked nanoribbons are also observed (Fig. 5C). What's more, the HRTEM image of the Cu₂O/THPP composite is taken and shown in Fig. 5D. The lattice fringes with a spacing of 0.304 nm are clearly observed, which can be indexed as the (110) crystal plane of cubic phase Cu₂O [30]. Surprisingly, the crystal planes attributed to Cu(OH)₂ observed in the XRD (Fig. 4A) cannot be seen in the HRTEM image of the Cu₂O/THPP composite. It is probably due to the different response of Cu₂O and Cu(OH)₂ to the bombardment of

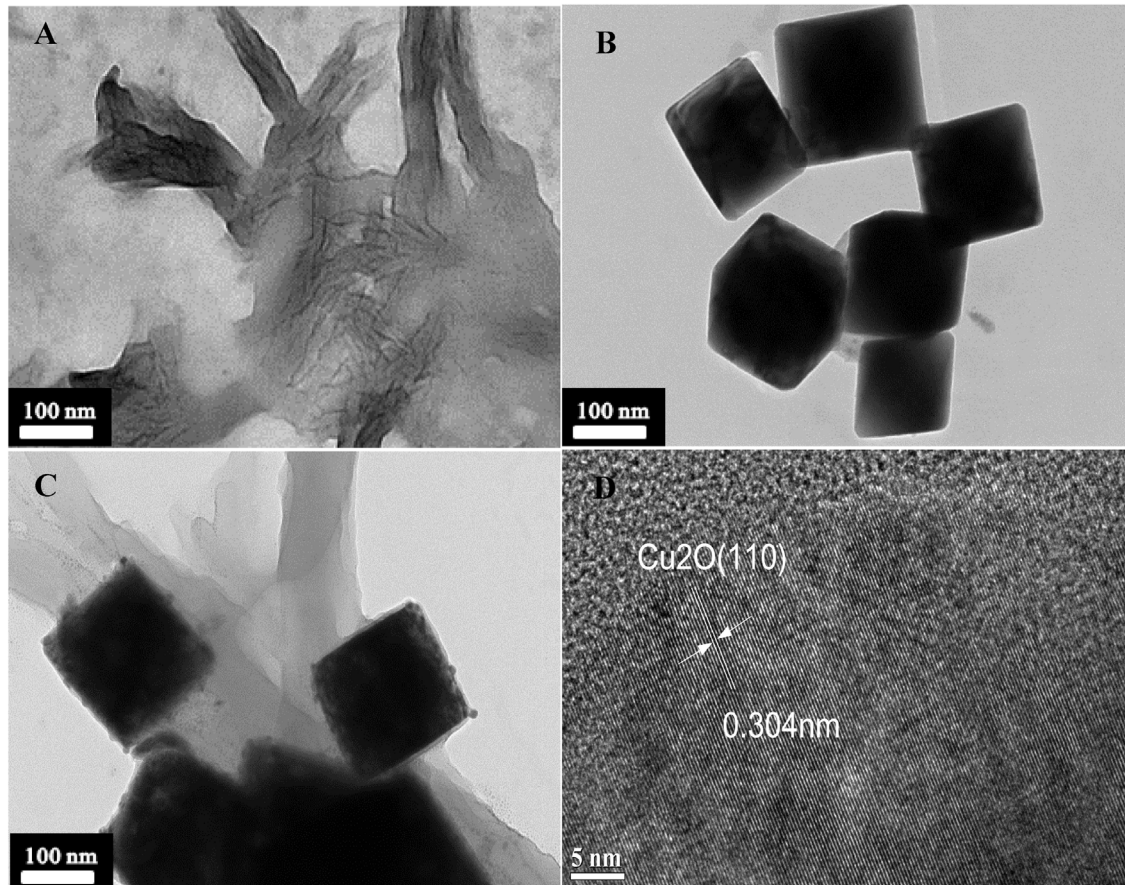


Fig. 5. TEM images for THPP (A), Cu₂O (B), 25%Cu₂O/THPP (C) and HRTEM image for 25%Cu₂O/THPP (D).

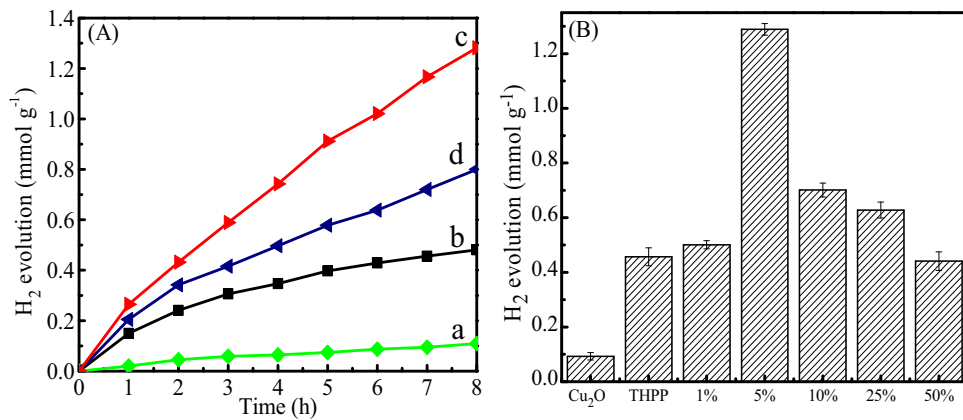


Fig. 6. (A) The relationship between the amount of H₂ evolved and irradiation time over various photocatalysts. a: Cu₂O; b: THPP; c: 5%Cu₂O/THPP; d: 5%Cu₂O/TPP. (B) The dependence of hydrogen evolved on the content of Cu₂O in the composite (irradiated for 8 h).

electron beams [31]. It is known that Cu(OH)₂ is easy to be decomposed above 20 °C. Therefore, it is deduced that a small amount of Cu(OH)₂ on the surface of the Cu₂O could be decomposed under the bombardment of electron beams with high energy.

In addition, TEM image of the Cu₂O/TPP composite was also taken (Fig. S4), it is found that, besides blurred cubic Cu₂O, separated TPP aggregates can be observed, which is different from the image of the Cu₂O/THPP. The result further confirms that the some hydroxyl groups in THPP react with Cu₂O by hydrogen bond and/or electrostatic interaction, besides coordination interaction. Otherwise, the wrapped Cu₂O could not be observed in the TEM image of the Cu₂O/THPP composite (Fig. 5C). The result of TEM coincides with those of UV-vis spectra and FTIR, which further confirms the deduction shown in Scheme 1. The close combination between THPP and Cu₂O will facilitate the electron transfer from THPP to Cu₂O, which is profitable to inhibit the recombination of electron/hole pairs and to improve the photocatalytic activity.

3.3. Photocatalytic performance for hydrogen evolution

As shown in Fig. 6A, under the same conditions, the activity of hydrogen evolution over pure Cu₂O or THPP is low. However, after introducing 5% Cu₂O into THPP, the activity of hydrogen evolution over the composite is dramatically improved, and the activity is about 2.3 times higher than the summation of the activity of Cu₂O and THPP. It is indicated that there exists the synergistic effect between Cu₂O and THPP in the composite. Moreover, the catalytic activity of the target product (Cu₂O/THPP) is higher than that of the Cu₂O/TPP composite. It is demonstrated that the combination mode

and the interaction strength have important influence on the performance of Cu₂O/porphyrin composites. Furthermore, as is shown in Fig. 6B, the activity of hydrogen evolved is the highest when the content of Cu₂O in the composite is 5%. It is deduced that, when the Cu₂O is less than 5%, more aggregation among THPP molecules would take place, which could inhibit the electron transfer. While the recombination of electron and hole would increase when the amount of Cu₂O in the composite is beyond 5%.

3.4. Electron transfer and photocatalytic mechanism for the Cu₂O/THPP composite

In generally, the production and the separation of photogenerated charge carries (electron/hole pairs) can be easily demonstrated from fluorescence spectra. In order to deeply understand the interaction between Cu₂O and THPP in the composite, fluorescence spectra are measured and shown in Fig. 7.

For THPP, there exist two emission peaks at 681 nm and at 738 nm, respectively. After interacting with Cu₂O, the emission peaks are quenched (Fig. 7A), and the peak at 723 nm is blue-shifted 15 nm. Compared fluorescence spectrum of THPP with those of CuTHPP and Cu₂O/THPP, the fluorescence is quenched more greatly in the Cu₂O/THPP. It is deduced that the weakened fluorescence partially comes from heavy-atom effect of Cu ions coordinated to THPP, and is mainly attributed to intermolecular electron transfer from THPP to Cu₂O according to the greatly quenched fluorescence and the movement of the peak at 723 nm [32]. Differently, after introducing Cu₂O into TPP, two blue-shifted emission peaks are observed, which suggests that the TPP

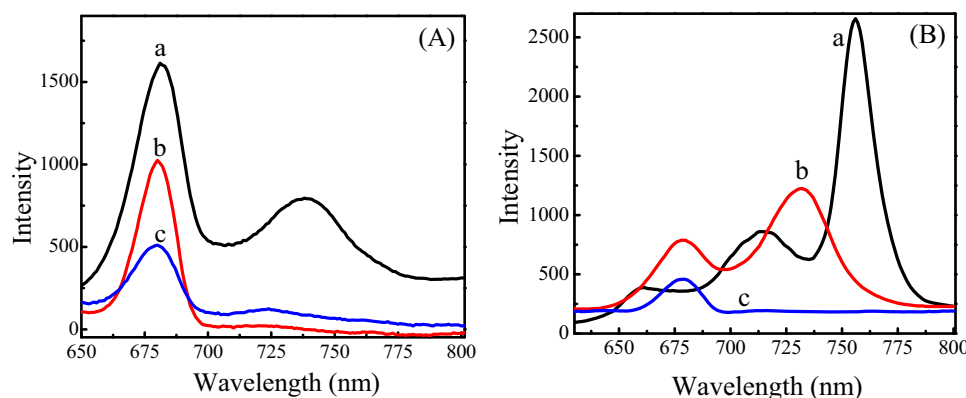


Fig. 7. (A) Fluorescence spectra of THPP (a), CuTHPP (b) and 5% Cu₂O/THPP (c). (B) Fluorescence spectra of TPP (a), 5% Cu₂O/TPP (b) and CuTPP (c). $\lambda_{ex} = 450$ nm.

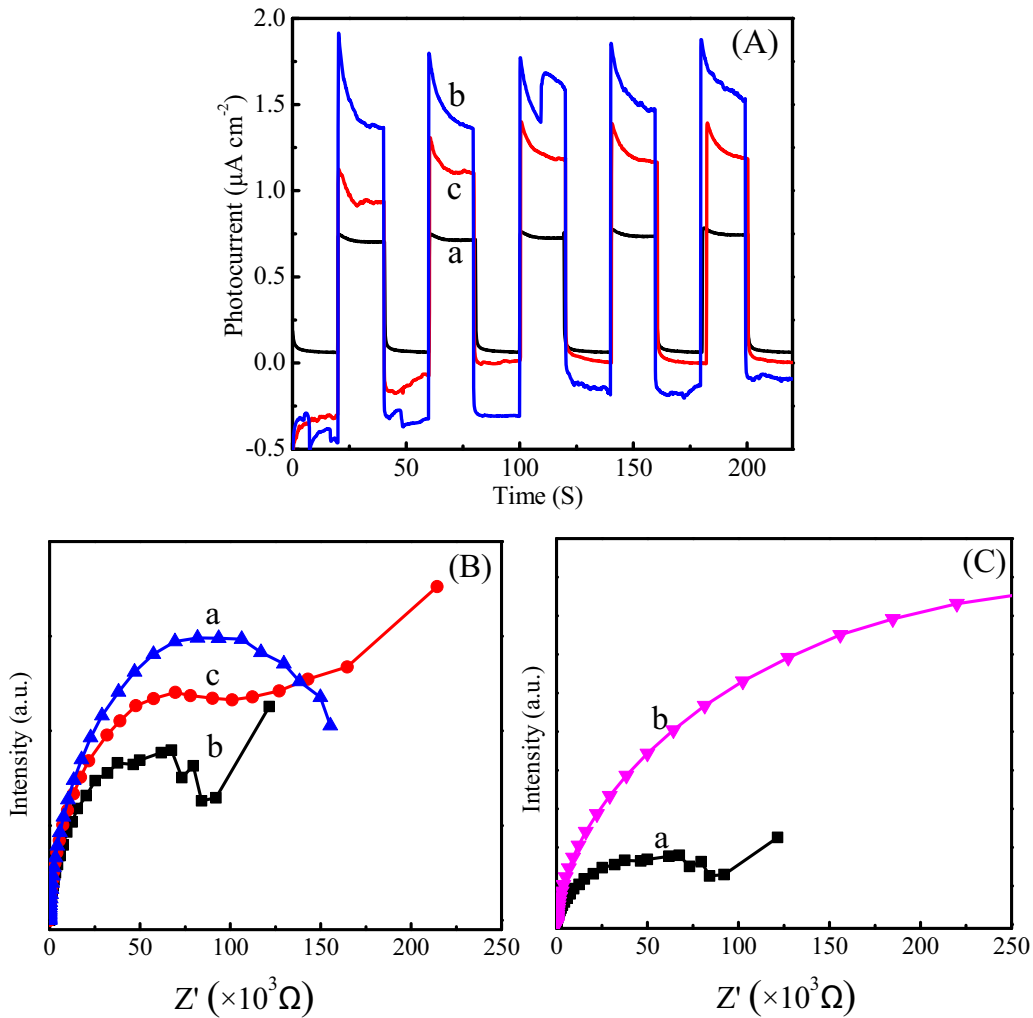


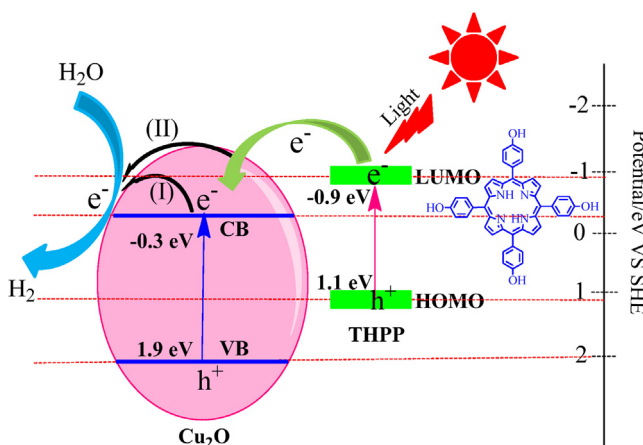
Fig. 8. A Photocurrent response of THPP (a), 5%Cu₂O/THPP (b) and 25%Cu₂O/THPP (c). B: Nyquist plots of electrochemical impedance spectra of THPP (a), 5%Cu₂O/THPP (b) and 25%Cu₂O/THPP (c). C: Nyquist plots of electrochemical impedance spectra of 5% Cu₂O/TPP (a) and 5% Cu₂O/THPP (b). The measurements were performed in 0.5 mol L⁻¹ Na₂SO₄ aqueous solution.

molecules in the Cu₂O/TPP composite adopt sitting-atop configuration where the energy difference between lowest unoccupied molecular orbital (LUMO) and highest occupied molecular orbital (HOMO) is higher than TPP [33–36]. Moreover, compared the fluorescence difference of Cu₂O/THPP composite and CuTHPP with that of Cu₂O/TPP composite and CuTPP, the more fluorescence quench is observed in the Cu₂O/THPP composite. The difference for the Cu₂O/THPP composite and the Cu₂O/TPP composite could come from the different interaction between the porphyrin (THPP/TPP) and Cu₂O. The result demonstrates that the aggregation among THPP molecules is reduced greatly due to the stronger interaction between Cu₂O and THPP. Therefore, the separation of electron/hole pairs is facilitated due to the special binding mode between Cu₂O and THPP, which is beneficial to improve the photocatalytic activity of the Cu₂O/THPP composite.

In order to further study the interfacial electron transfer in the composite, photocurrent response and electrochemical impedance spectra of some as-prepared composites are measured. All transient photocurrent curves show a quick response once the light turns on, because of electrons in samples gathered before the light switches. As shown in Fig. 8A, the photocurrent of the THPP improves obviously after introducing Cu₂O. It could be attributed to the decreased recombination of electron/hole pairs in the Cu₂O/THPP heterojunction structures. This confirms the special binding mode

(hydrogen bond, electrostatic interaction and coordination interaction) between THPP and Cu₂O is effectively way to enhance the photocurrent intensity. The transient photocurrent curves of the Cu₂O/THPP are not smooth, and there is a specific decay during the illumination period because of the photogenerated charge carriers accumulated before the light turns on [1,37]. In practical terms, the photogenerated charge carriers were concentrated during the continued light illumination.

Furthermore, as can be seen from electrochemical impedance spectra of as-prepared composites (Fig. 8B), the semicircle diameter of the THPP becomes small after introducing Cu₂O. It is the characteristics that the interfacial resistance decreases. That is to say, Cu₂O can efficiently facilitate the photoproduced electron transfer of the THPP. As can be seen in Fig. 8C, the interfacial resistance of the Cu₂O/THPP composite is far less than that of the Cu₂O/TPP composite (The different scope is given in Fig. 8(B) and (C), respectively, in order to show completely the electrochemical impedance spectra of 5% Cu₂O/TPP). The close combination and the stronger interaction between Cu₂O and THPP (have been proved by fluorescence spectra and TEM image) could be the reason that higher electron transfer efficiency and smaller interfacial resistance are shown in the Cu₂O/THPP composite, which is very beneficial to enhance the photocatalytic activity of the Cu₂O/THPP composite.



Scheme 2. Mechanism scheme for the photoproduced electron transfer and hydrogen production from water reduction in the $\text{Cu}_2\text{O}/\text{THPP}$ composite.

According to the results of photocatalytic performance, fluorescence spectra, photocurrent response and electrochemical impedance spectra, a possible mechanism for photoproduced electron transfer and hydrogen production from water reduction is suggested and shown in **Scheme 2**. Differently from photocatalytic degradation, before photocatalytic hydrogen evolution, it was evacuated by a vacuum pump in order to remove the air in the system. Therefore, there does not exist $\cdot\text{OH}$ and $\text{O}_2\cdot^-$ in the system. In addition, the energy of the lowest unoccupied molecular orbital (LUMO) for the THPP [38] is higher than that of the Cu_2O [1] (when the size of the particle is bigger than 10 nm, morphology and size of Cu_2O have less influence on the band gap (2.0–2.2 eV) and the position of its CB and VB [39]), which is conducive to the photo-induced electron transfer from THPP to Cu_2O [40]. After visible light irradiation, THPP is photoexcited, and the photo-excited electrons from THPP are easily transferred towards Cu_2O and injected into the conduct band of Cu_2O , which inhibits recombination of photo-generated electron/hole pairs. It can be easily confirmed from fluorescence spectra (Fig. 7A). Of course, Cu_2O can also be photoexcited. The photoproduced electrons produced are captured by water molecules, and then the water molecules are reduced into H_2 (Fig. 6), and the holes are consumed by the sacrifice agent (triethanolamine).

Using the 5% $\text{Cu}_2\text{O}/\text{THPP}$ nanocomposite as the photocatalyst, cycling measurements of hydrogen evolution through photocatalytic water reduction are shown in **Fig. 9**. In each recycle, the reaction system is evacuated and irradiated for 6 h. It can be seen

that, in the second recycle, the amount of hydrogen evolution over the composite is slightly decreased, and the amount of hydrogen evolution is hardly changed from the third time. According to the result of FTIR, though the band at 966 cm^{-1} becomes weak gradually followed with increasing Cu_2O in the composite, the band did not disappear completely. It is indicated that a few THPP did not coordinate with Cu^+ , but interacted with Cu_2O by hydrogen bond and/or electrostatic interaction. In the process of photocatalytic hydrogen evolution, these THPP could be taken off from Cu_2O surface under the weak basic condition [41] (Measurement of photocatalytic activity was performed in 10 vol.% triethanolamine (TEA) aqueous solution, and the pH value is about 8–9). As a result, the amount of hydrogen evolution produced over the composite is slightly decreased in the second recycle. Due to the lost of the THPP linked weakly with Cu_2O , the pH value of the solution is slightly decreased. When the pH value is close to neutral, the THPP molecules, especially those linked strongly on Cu_2O , were not taken off any more. Therefore, the amount of hydrogen evolution is hardly changed from the third cycle to the fifth cycle, which suggests that the composite photocatalyst is relatively stable.

4. Conclusions

A novel $\text{Cu}_2\text{O}/\text{THPP}$ nanocomposite with special structure was achieved by a facile process. The assembly mechanism of Cu_2O and THPP was explored. The result showed that hydrogen bond, electrostatic interaction and coordination interaction were the main driving forces for the assembly of Cu_2O and THPP. Furthermore, photocatalytic activity for hydrogen evolution over the $\text{Cu}_2\text{O}/\text{THPP}$ nanocomposite was investigated. The composite showed higher photocatalytic performance than pure Cu_2O , THPP or $\text{Cu}_2\text{O}/\text{TPP}$. Mechanisms of the electron transfer and hydrogen evolution were explored by various means. It was demonstrated that the synergistic effect, and strong interaction between THPP and Cu_2O were the important factors affected on photocatalytic activity. Consequently, the composite of Cu_2O and THPP is an efficient approach for preparing cheap metal oxides/porphyrin based photocatalyst with higher photocatalytic activity. It could also helpful to understand the interaction mechanism among constituents in the composite catalysts.

Acknowledgements

This work was financially supported by the Innovation Program of Shanghai Municipal Education Commission (No. 15ZZ096), and the National Natural Science Foundation of China (No. 21301118, 21305092 and 21371070).

Appendix A. Supplementary data

Supplementary data associated with this article can be found, in the online version, at <http://dx.doi.org/10.1016/j.apcatb.2017.04.056>.

References

- [1] J. Zhang, H.P. Ma, Z.F. Liu, Highly efficient photocatalyst based on all oxides $\text{WO}_3/\text{Cu}_2\text{O}$ heterojunction for photoelectrochemical water splitting, *Appl. Catal. B Environ.* 201 (2017) 84–91.
- [2] M.S. Yao, W.X. Tang, G. Wang, B. Nath, G. Xu, MOF thin film-coated metal oxide nanowire array: significantly improved chemiresistor sensor performance, *Adv. Mater.* 28 (2016) 5229–5234.
- [3] Y. Li, B. Wang, S. Liu, X. Duan, Z. Hu, Synthesis and characterization of $\text{Cu}_2\text{O}/\text{TiO}_2$ photocatalysts for H_2 evolution from aqueous solution with different scavengers, *Appl. Surf. Sci.* 324 (2015) 736–744.
- [4] J. He, B. Hu, Y. Zhao, Superaerobic electrode with metal@metal-oxide powder catalyst for oxygen evolution reaction, *Adv. Funct. Mater.* 26 (2016) 5998–6004.
- [5] P.D. Tran, S.K. Batabyal, S.S. Pramana, J. Barber, L.H. Wong, S.C.J. Loo, A cuprous oxide-reduced graphene oxide ($\text{Cu}_2\text{O}-\text{rGO}$) composite photocatalyst for

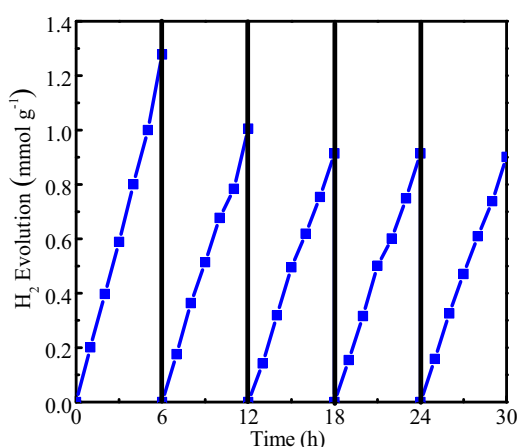


Fig. 9. Cycling measurements of hydrogen evolution through photocatalytic water reduction using the 5% $\text{Cu}_2\text{O}/\text{THPP}$ nanocomposite as the photocatalyst.

hydrogen generation employing rGO as an electron acceptor to enhance the photocatalytic activity and stability of Cu_2O , *Nanoscale* 4 (2012) 3875–3878.

[6] M.A. Mahmoud, W. Qian, M.A. El-Sayed, Following charge separation on the nanoscale in Cu_2O -Au nanoframe hollow nanoparticles, *Nano Lett.* 11 (2011) 3285–3289.

[7] P.E. De Jongh, D. Vanmaekelbergh, J.J. Kelly, Cu_2O a catalyst for the photochemical decomposition of water? *Chem. Commun.* 106 (1999) 1069–1070.

[8] L. Jian, D. Cai, G. Su, D. Lin, M. Lin, J. Li, The accelerating effect of silver ion on the degradation of methyl orange in Cu_2O system, *Appl. Catal. A Gen.* 512 (2015) 74–84.

[9] H. Jia, R. Roa, S. Angioletti-Uberti, K. Henzler, A. Ott, X.Z. Lin, J. Möser, Z. Kochovski, A. Schnegg, J. Dzubiella, M. Ballauff, Y. Lu, Thermosensitive Cu_2O -PNIPAM core-shell nanoreactors with tunable photocatalytic activity, *J. Mater. Chem. A* 4 (2016) 9677–9684.

[10] J.Y. Ho, M.H. Huang, Synthesis of submicrometer-sized Cu_2O crystals with morphological evolution from cubic to hexapod structures and their comparative photocatalytic activity, *J. Phys. Chem. C* 113 (2009) 14159–14164.

[11] M. Yamamoto, L. Wang, F.S. Li, T. Fukushima, K. Tanaka, L.C. Sun, H. Imahori, Visible light-driven water oxidation using a covalently-linked molecular catalyst-sensitizer dyad assembled on a TiO_2 electrode, *Chem. Sci.* 7 (2016) 1430–1439.

[12] M.A.M. Vásquez, S.A. Suárez, F. Doctorovich, Gold and silver anchored cobalt porphyrins used for catalytic water splitting, *Mater. Chem. Phys.* 159 (2015) 159–166.

[13] R. Marczak, F. Werner, J.F. Gnichwitz, A. Hirsch, D.M. Guldi, W. Peukert, Communication via electron and energy transfer between zinc oxide nanoparticles and organic adsorbates, *J. Phys. Chem. C* 113 (2009) 2460–2462.

[14] P. Bhyrappa, Scott R. Wilson, Kenneth S. Suslick, Hydrogen-bonded porphyrinic solids: supramolecular networks of octahydroxy porphyrins, *J. Am. Chem. Soc.* 119 (1997) 8492–8502.

[15] G. Lu, X. Zhang, X. Cai, J. Jiang, Tuning the morphology of self-assembled nanostructures of amphiphilic tetra(p-hydroxyphenyl)porphyrins with hydrogen bonding and metal-ligand coordination bonding, *J. Mater. Chem.* 19 (2009) 2417–2424.

[16] J.D. Megiatto, D.I. Schuster, S. Abwandner, G.D. Miguel, D.M. Guldi, [2] Catenanes decorated with porphyrin and [60] fullerene groups: design, convergent synthesis, and photoinduced processes, *J. Am. Chem. Soc.* 132 (2010) 3847–3861.

[17] G. Lu, X. Zhang, X. Cai, J. Jiang, Tuning the morphology of self-assembled nanostructures of amphiphilic tetra(p-hydroxyphenyl)porphyrins with hydrogen bonding and metal-ligand coordination bonding, *J. Mater. Chem.* 19 (2009) 2417–2424.

[18] Z.Q. Zhang, L.Y. Kong, Y. Xiong, Y. Luo, J. Li, The synthesis of $\text{Cu}(\text{II})$ $\text{Zn}(\text{II})$, and $\text{Co}(\text{II})$ metalloporphyrins and their improvement to the property of Li/SOCl_2 battery, *J. Solid State Electr.* 18 (2014) 3471–3477.

[19] L.A. Andersson, C. Sotiriou, C.K. Chang, T.M. Loehr, Facile lactonization and inversion of vicinal diols in heme d-type chlorins a spectroscopic study, *J. Am. Chem. Soc.* 109 (1987) 258–264.

[20] W.C. Huang, L.M. Lyu, Y.C. Yang, M.H. Huang, Synthesis of Cu_2O nanocrystals from cubic to rhombic dodecahedral structures and their comparative photocatalytic activity, *J. Am. Chem. Soc.* 134 (2012) 1261–1267.

[21] E. Vargas, R. Vargas, O. Núñez, A TiO_2 surface modified with copper (II) phthalocyanine-tetrasulfonic acid tetrasodium salt as a catalyst during photoinduced dichlorvos mineralization by visible solar light, *Appl. Catal. B Environ.* 156–157 (156) (2014) 8–14.

[22] G. Rojas, X. Chen, C. Bravo, J.H. Kim, J.S. Kim, J. Xiao, P.A. Dowben, Y. Gao, X.C. Zeng, W. Choe, A. Enders, Self-assembly and properties of nonmetalated tetraphenyl-porphyrin on metal substrates, *J. Phys. Chem. C* 114 (2010) 9408–9415.

[23] A. Verdini, P. Shinde, G.L. Montanari, S.T. Suran-Brunelli, M. Caputo, G.D. Santo, C.A. Pignedoli, L. Floreano, D. Passerone, A. Goldon, Water formation for the metalation of porphyrin molecules on oxidized $\text{Cu}(111)$, *Chem. Eur. J.* 22 (2016) 14672–14677.

[24] P. Asen, S. Shahrokhian, A high performance supercapacitor based on graphene/polypyrrole/ Cu_2O - $\text{Cu}(\text{OH})_2$ ternary nanocomposite coated on nickel foam, *J. Phys. Chem. C* 121 (2017) 6508–6519.

[25] J. He, B.B. Hu, Y. Zhao, Superaerophobic electrode with metal@metal-oxide powder catalyst for oxygen evolution reaction, *Adv. Funct. Mater.* 26 (2016) 5998–6004.

[26] S. Joshi, S.J. Ippolito, M.V. Sunkara, Convenient architectures of $\text{Cu}_2\text{O}/\text{SnO}_2$ type II p-heterojunctions and their application in visible light catalytic degradation of rhodamine B, *RSC Adv.* 6 (2016) 43672–43684.

[27] J.P. Espinós, J. Morale, A. Barranco, A. Caballero, J.P. Holgado, A.R. González-Elipe, Interface effects for Cu/CuO , and Cu_2O deposited on SiO_2 and ZrO_2 , XPS determination of the valence state of copper in Cu/SiO_2 and Cu/ZrO_2 catalysts, *J. Phys. Chem.* 106 (2002) 6921–6929.

[28] J. Xiao, S. Ditze, M. Chen, F. Buchner, M. Stark, M. Drost, H.-P. Steinrück, J.M. Gottfried, H. Marbach, Temperature-dependent chemical and structural transformations from 2H-tetraphenylporphyrin to copper(II)-tetraphenylporphyrin on $\text{Cu}(111)$, *J. Phys. Chem. C* 116 (2012) 12275–12282.

[29] M. Shirakawa, S.I. Kawano, N. Fujita, K. Sada, S. Shinkai, Hydrogen-bond-assisted control of H versus J aggregation mode of porphyrins stacks in an organogel system, *J. Org. Chem.* 68 (2003) 5037–5044.

[30] S. Ren, B. Wang, H. Zhang, P. Ding, Q. Wang, A sandwiched $\text{ZnO}@\text{Au}@\text{Cu}_2\text{O}$ nanorod films as efficient visible-light-driven plasmonic photocatalysts, *Appl. Mater. Interfaces* 7 (2015) 4066–4074.

[31] X.Q. Li, L.E. Zhang, J. Mu, J.L. Qiu, Fabrication and properties of porphyrin nano- and microparticles with novel morphology, *Nanoscale Res. Lett.* 3 (2008) 169–178.

[32] M. Makarska-Bialokoz, Spectroscopic evidence of xanthine compounds fluorescence quenching effect on water-soluble porphyrins, *J. Mol. Struct.* 1081 (2015) 224–232.

[33] O. Horváth, R. Huszánk, Z. Valicsek, G. Lendvay, Photophysics and photochemistry of kinetically labile, water-soluble porphyrin complexes, *Coordin. Chem. Rev.* 250 (2006) 1792–1803.

[34] J. Schneider, F. Kollhoff, J. Bernardi, A. Kaftan, J. Libuda, T. Berger, M. Laurin, O. Diwald, Porphyrin metalation at the MgO nanocube/toluene interface, *ACS Appl. Mater. Interface* 7 (2015) 22962–22969.

[35] O. Horváth, Z. Valicsek, A. Vogler, Unique photoreactivity of mercury(II) 5,10,15,20-tetrakis(4-sulfonatophenyl)porphyrin, *Inorg. Chem. Comm.* 7 (2004) 854–857.

[36] S.M.B. Aly, M. Eita, J.I. Khan, E. Alarousu, O.F. Mohammed, Remarkable fluorescence enhancement versus complex formation of cationic porphyrins on the surface of ZnO nanoparticles, *J. Phys. Chem. C* 118 (2014) 12154–12161.

[37] S.G. Kumar, L.G. Devi, Review on modified TiO_2 photocatalysis under UV/visible light: selected results and related mechanisms on interfacial charge carrier transfer dynamics, *J. Phys. Chem. A* 115 (2011) 13211–13241.

[38] L. Smykalla, P. Shukryna, C. Mende, T. Rüffer, H. Lang, M. Hietzhold, Manipulation of the electronic structure by reversible dehydrogenation of tetra(p-hydroxyphenyl)porphyrin molecules, *Surf. Sci.* 628 (2014) 92–97.

[39] M. Sabbaghian, J. Beheshtian, R.N. Liarjdame, Preparation of Cu_2O nanostructures by changing reducing agent and their optical properties, *Mater. Lett.* 153 (2015) 1–4.

[40] Y.J. Chen, H. Ge, L. Wei, Z.H. Li, R.S. Yuan, P. Liu, X.Z. Fu, Reduction degree of reduced graphene oxide (RGO) dependence of photocatalytic hydrogen evolution performance over $\text{RGO}/\text{ZnIn}_2\text{S}_4$ nanocomposites, *Catal. Sci. Technol.* 3 (2013) 1712–1717.

[41] Y.J. Yuan, J.R. Tu, Z.J. Ye, H.W. Lu, Z.G. Ji, B. Hu, Y.H. Li, D.P. Cao, Z.T. Yu, Z.G. Zou, Visible-light-driven hydrogen production from water in a noble-metal-free system catalyzed by zinc porphyrin sensitized MoS_2/ZnO , *Dyes Pigm.* 123 (2015) 285–292.